Electronic Supplementary Material (ESI) for Journal of Materials Chemistry C.

Electronic Supplementary Information

Efficient Charge Transfer in Solution-Processed PbS Quantum Dot-Reduced Graphene Oxide Hybrid Materials

*Beatriz Martín-García,[a,b] Anatolii Polovitsyn,[a,c] Mirko Prato[a] and Iwan Moreels[a,b]**

[a] NanoChemistry Department, Istituto Italiano di Tecnologia, Via Morego 30, IT-16163 Genova, Italy
[b] Graphene Labs, Istituto Italiano di Tecnologia, Via Morego 30, IT-16163 Genova, Italy
[c] Department of Physics, University of Genoa, Via Dodecaneso 33, IT-16146 Genova, Italy

1. XPS analysis of GO and rGO.

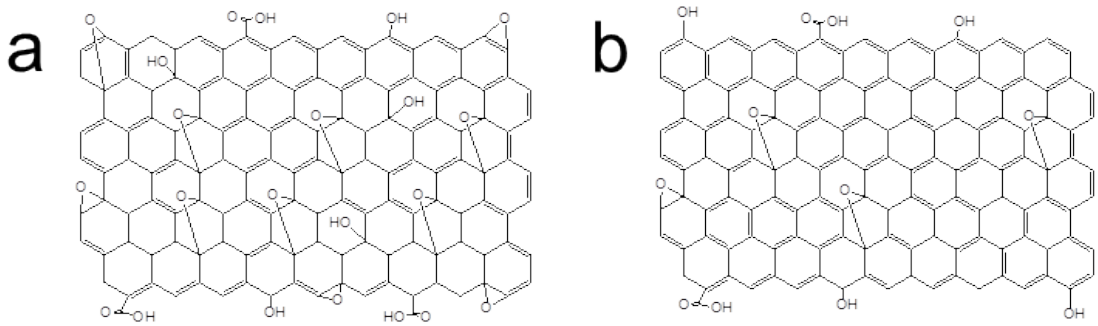

Scheme S1. Representative sketches of GO (a) and rGO (b) based on the Lerf-Klinowski model.[1]

XPS C_{1s} core-level spectra of GO and rGO are shown in Fig. S1a and b. To evaluate the reduction efficiency we relied on the atomic O/C ratio (see main text). Data are in line with the observed increased fraction of C sp^2 domains, from 41.5% in GO to 56.2% in rGO, respectively.

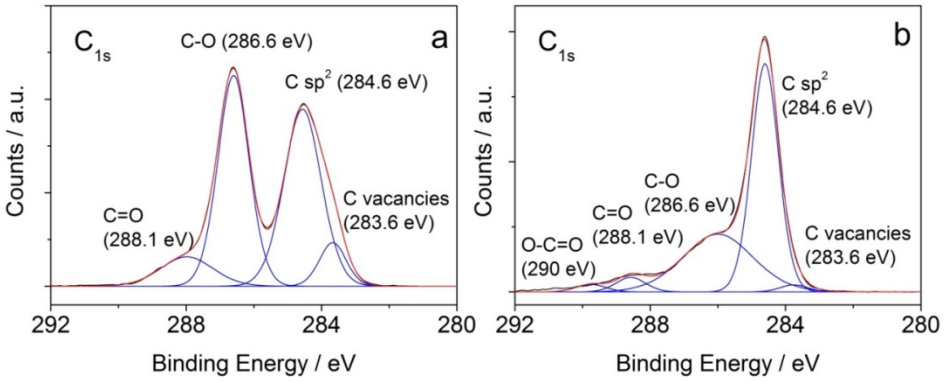

Fig. S1. XPS core-level C_{1s} spectra of GO (a) and rGO (b).

2. Functionalization of the graphene-based materials: molecular structures of linkers and ligands

In Fig. S2 we show the molecular structures of the different molecules used in this work for the QD surface modification and rGO functionalization: ATP, ABA, MPTS and MUA.

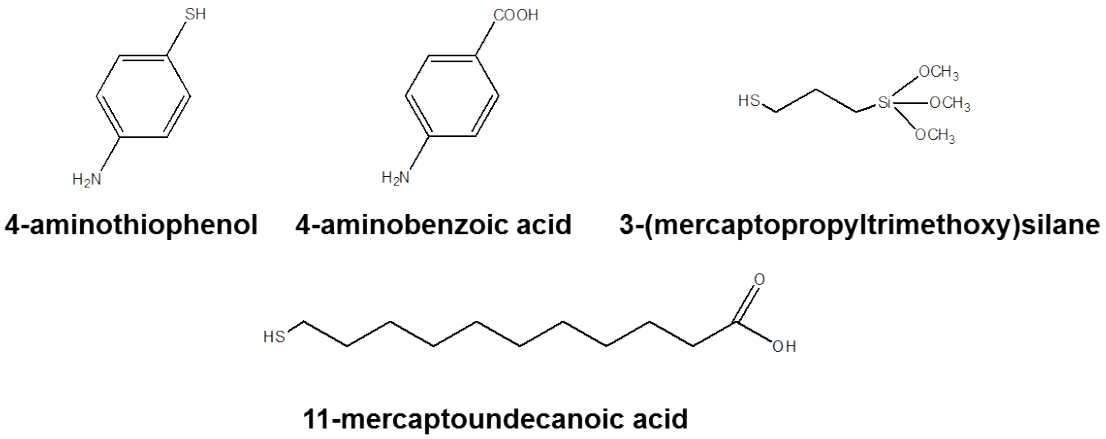

Fig. S2. Structure of the different molecules used.

3. XPS analysis of ATP and ABA functionalized rGO and TEM images for the QDs coupling results.

XPS spectra of the rGO samples functionalized with ATP and ABA are shown in Fig. S3a-d. Both functionalization approaches lead to the formation of an amide bond (peak at 400.3 eV, N_{1s} core-level spectrum, Fig. S3c) between the aromatic ring and the rGO, leaving the corresponding thiol of ATP (Fig. S3d) and carboxylic group of ABA exposed. This bonding is also supported by the appearance of a C-N peak at 285.6 eV in the C_{1s} core level spectra (Fig. S3a-b). The comparable N/C and S/C ratios show that the functionalization achieved in both cases is similar. We also observed the nitrate peak in the corresponding N_{1s} core-level spectrum (Fig. S3c) and a plasmon loss peak of the Si substrate in the S_{2p} core-level spectrum (Fig. S3d). However, these are unrelated to the ABA and ATP molecules, respectively, as the nitrate (NO_3^-) peak likely remains from the production of GO where $NaNO_3$ was used, or from the $NaNO_2$ added in the functionalization reaction.[2, 3] Therefore, they are not considered in the determination of the rGO degree of functionalization. The low coverage achieved with both ABA and ATP (N/C atomic ratio of 0.02) is also reflected by the assembly of the QDs on the ABA- or ATP-*f*- rGO sheets (Fig. S3e), where QDs are found mainly along edges and ridges.

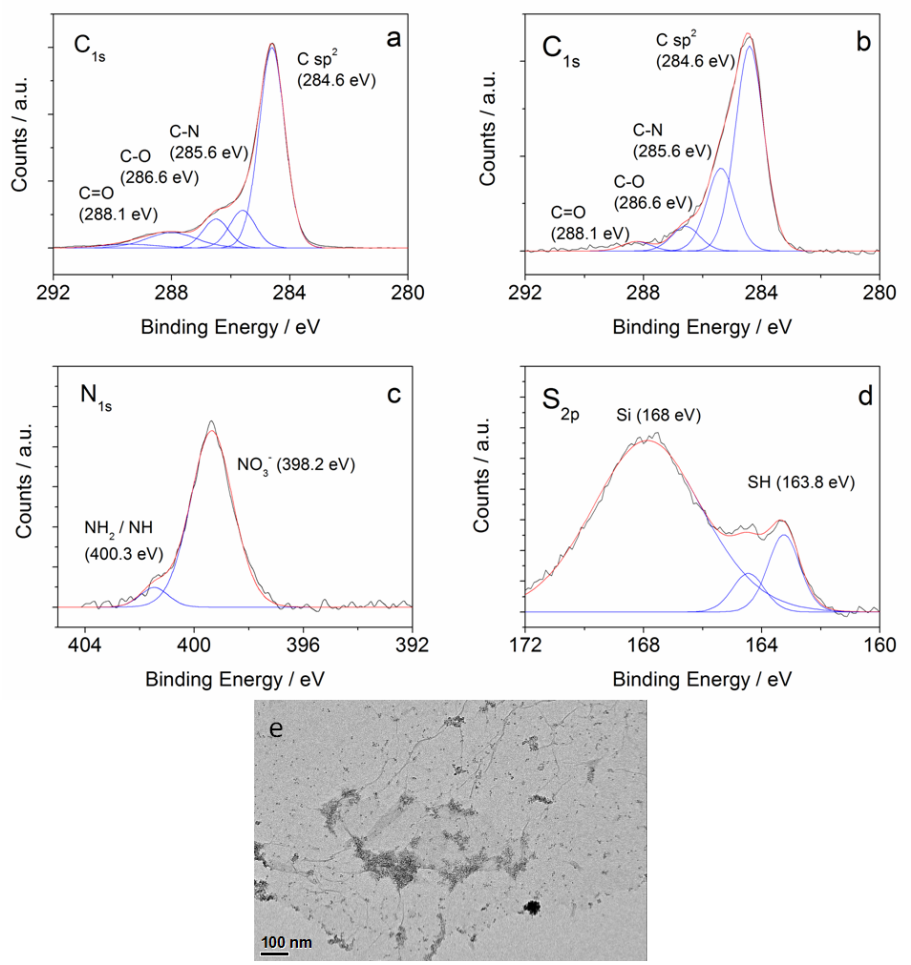

Fig. S3. XPS core-level C_{1s} spectra of ABA-*f*-rGO (a) and ATP-*f*-rGO (b). XPS core-level N_{1s} and S_{2p} spectra of ABA-*f*-rGO (c) and ATP-*f*-rGO (d), respectively. (e) Representative TEM image of core PbS QDs (5.0 nm diameter)/ABA-*f*-rGO.

4. Silane-functionalization and QD coupling in GO.

We evaluated the GO degree of functionalization achieved using MPTS by quantitative XPS analysis of the S/C and Si/C atomic ratios (Fig. S4), obtaining an average ratio of 0.15. Thus, also in the case of GO we increased the degree of functionalization with regards to ABA or ATP. As in the case of silane-*f*-rGO presented in the main text, the best fit for the S_{2p} profiles in the silane-*f*-GO is obtained by using two components: (i) a minor component centered at 164.2 ± 0.2 eV, corresponding to 10 ± 2 % of the total amount of sulfur, which is related to disulfide bonds. (ii) A main component centered at 163.2 ± 0.2 eV, constituting 90 ± 2 % of the total signal, which corresponds to the thiol head group.

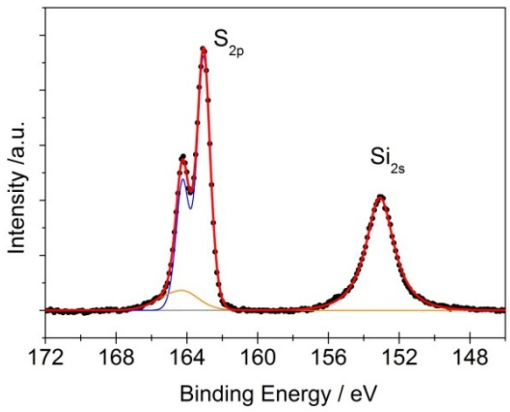

Fig. S4. XPS core-level S_{2p} and Si_{2s} spectra of silane-*f*-GO. The Si_{2s} peak is centered at (153.2±0.2) eV, a typical position for silanes. For the S_{2p} spectrum, the fitted curves correspond to unbound thiols (blue line) and disulfide (orange line).

The preparation procedure for coupling the QDs and silane-*f*-GO is the same as for silane-*f*-rGO. After attaching the QDs to the silane-*f*-GO sheets, the TEM images (Fig. S5) show that a well-controlled hybrid material is achieved, where the QDs cover exclusively the GO sheets.

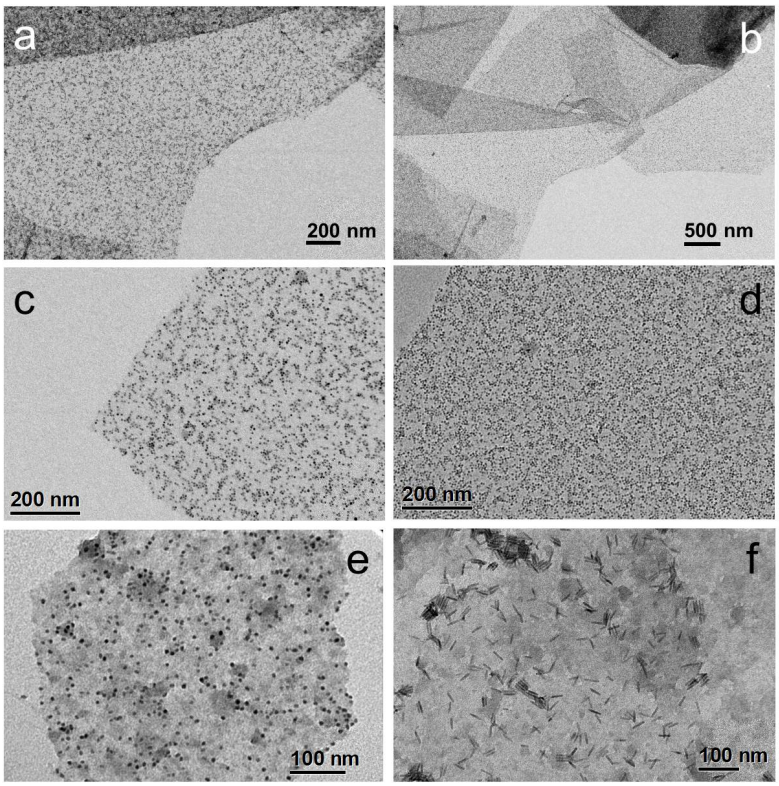

Fig. S5. (a-d) Representative TEM images of PbS QDs (5.0 nm diameter)/GO hybrid materials prepared from silane-*f*-GO. Comparison of the QD coverage achieved varying the QD/GO material ratio from 0.2 (c) to 0.8 (d) nmol QDs per µg GO. (e-f) Representative TEM images of hybrid materials prepared from silane-*f*-GO with different materials (e) CdSe QDs (5.8 nm) and (f) CdSe/CdS DIRs (28.3 nm length, 5.1 nm diameter).

From the QD PL dynamics analysis (Fig. S6) we observed that in the hybrid PbS QD/silane-*f*-GO a lower PL quenching, of up to 90%, and lifetime reduction from 1.4 µs (PbS QDs in TCE) to 178 ns (87% reduction) are achieved. Thus, the degree of reduction of the graphene-based material plays a role in the energy/charge transfer processes as discussed in the main text.

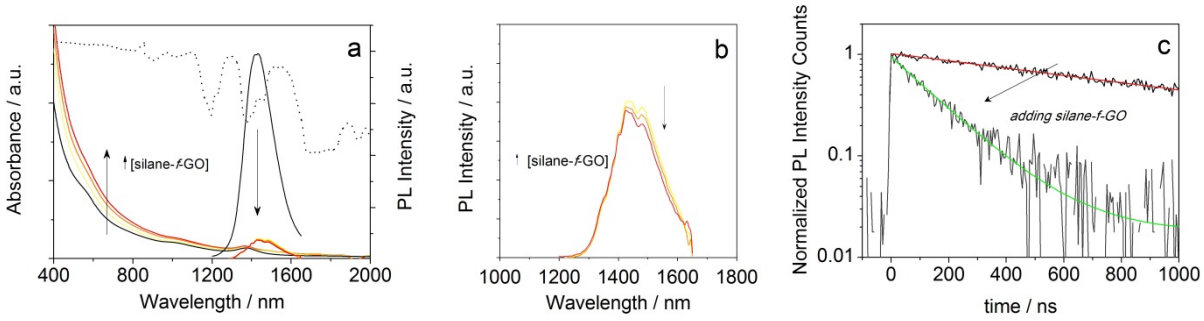

Fig. S6. Absorbance and PL (a, b) spectra of PbS QD/silane-*f*-GO hybrid materials dispersed in DMF with varying relative QD concentration (ratios 0.2, 0.4 and 0.8 nmol QDs per µg GO). The data from the reference, OA-capped PbS QDs in TCE, are shown as black lines. (c) Corresponding PL decay traces and fits for pure PbS QDs (red line) and PbS QD/silane-*f*-GO hybrid materials (green line) prepared with a relative concentration of 0.2 nmol per µg GO.

5. Estimation of the density of PbS QDs on the silane-*f*-(r)GO sheets.

To estimate the number of QDs attached on the surface of the (r)GO from TEM, we transformed experimental TEM images into a binary image (Fig. S7). The image is generated by applying a cutoff at an adequate intensity threshold, hereby separating the (r)GO background from the QDs. Then we evaluated the area occupied by the QDs and the surface of the underlying (r)GO sheet. The density of QDs is calculated as the total QD area divided by the area of the individual QDs (diameter 5.0 nm, area 19.6 nm^2). Table S1 presents the average obtained from the analysis of at least 4 TEM images at different scales for each sample.

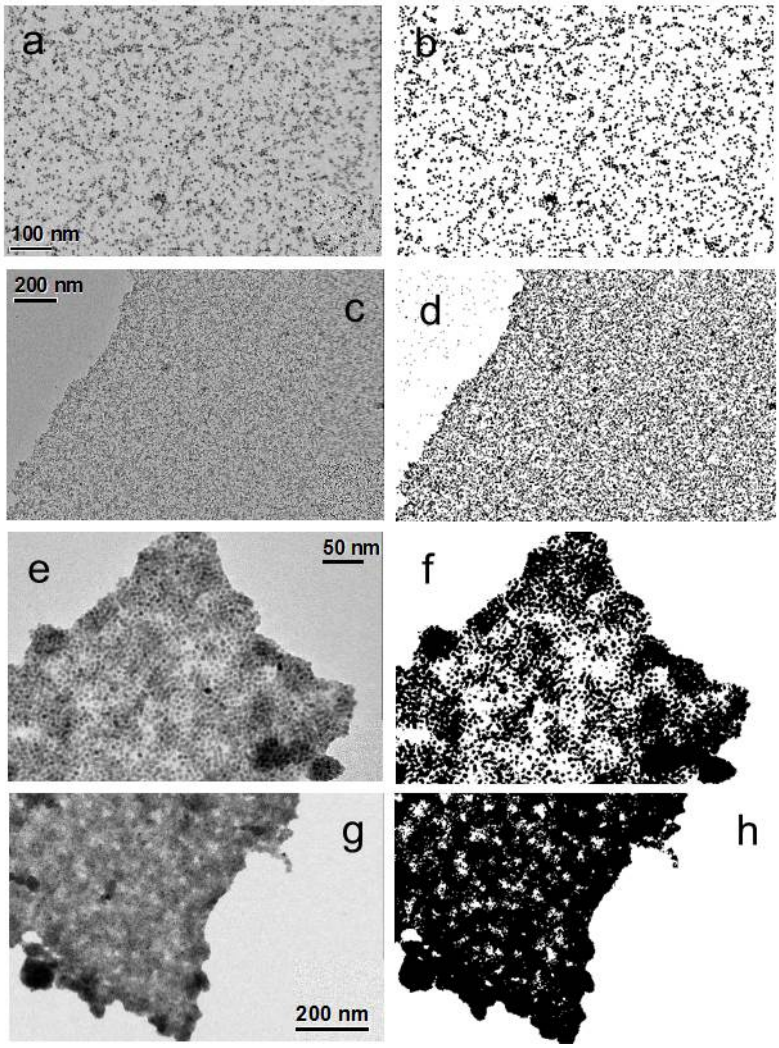

Fig. S7. Representative TEM images and the corresponding binary images of PbS QD/silane-*f*-(r)GO hybrid material at different QD/(r)GO ratios: on silane-*f*-GO with 0.2 (a, b) and 0.8 (c, d) nmol QDs per µg of GO, and on silane-*f*-rGO with 0.2 (e, f) and 0.8 (g, h) nmol QDs per µg of rGO.

Sample	nmol QDs per µg (r)GO	QDs per nm^2 of (r)GO
PbS QDs/silane-*f*-GO	0.2	0.009 ± 0.001
	0.8	0.014 ± 0.002
PbS QDs/silane-*f*-rGO	0.2	0.029 ± 0.004
	0.8	0.047 ± 0.002

Table S1. Data of the density of PbS QDs on silane-*f*-(r)GO sheets obtained from the TEM images analysis. Clearly, despite similar silane functionalization, the rGO sheets display a higher QD density.

6. Complementary control experiments

6.1. Ligand exchange and fluorescence spectroscopy characterization of MUA-capped PbS QDs.

In order to evaluate the effect of the thiol head group and the DMF solvent on the QDs PL emission properties, we prepared the QDs with an 11-mercaptoundecanoic acid (MUA) ligand shell. This molecule links in the same way as the silane and due to the exposed carboxylic head group, it allows dispersing the QDs in polar solvents such as DMF. To carry out the ligand exchange of OA with MUA we slightly adapted an experimental protocol already published.[6] Briefly, we added 1 mL of a 0.05 M MUA solution prepared in MeOH (0.1 M KOH, basic pH conditions) to a 100 µL toluene solution of OA-capped PbS QDs (45 µM).

From the time-resolved fluorescence decay (Fig. S8 and Table S2), we observed that the change of the ligand and solvent somewhat affect the QD PL emission properties, yet the exciton lifetime does not fall below 40-45% of the original value for MUA. Most importantly, the interaction of the QDs with the rGO promotes a much stronger reduction, and considering that in the case of the hybrid materials we do not replace all original OA ligands by thiols, we can assume that the inherent PL should be even less affected by ligand exchange, such that the PL quenching in the hybrid materials can be assigned to charge transfer to the rGO.

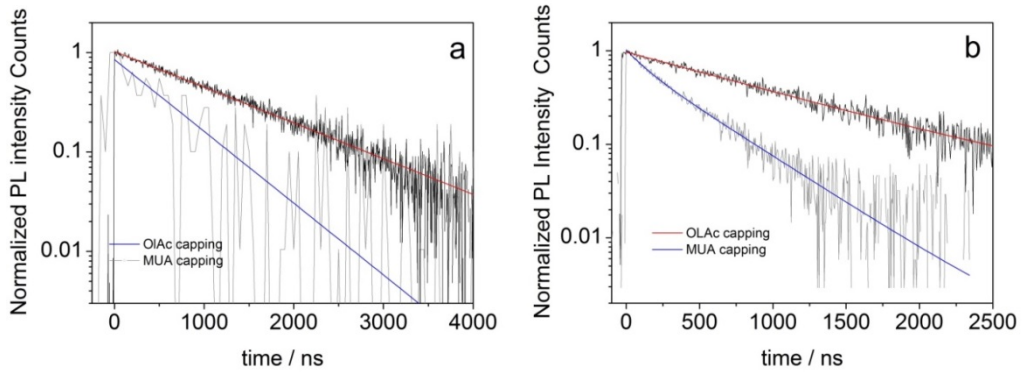

Fig. S8. PL decay traces of MUA-capped PbS QDs dispersed in DMF with regard to the original OA-capped PbS QDs for two different core size samples, *i.e.* 5.0 nm (a) and 5.6 nm (b). The OA-capped PbS QDs were dispersed in TCE, the ligand-exchanged samples in DMF.

Sample	Solvent	Ligand	τ_{eff} / µs
core PbS (5.0 nm)	TCE	OA	1.4
		MUA	0.63
core PbS (5.6 nm)	TCE	OA	0.99
		MUA	0.40

Table S2. Effective lifetime obtained from the fitting of the corresponding PL decay curves for the MUA-capped PbS QDs samples prepared in DMF.

6.2. EtOH washing effect on the QD PL emission properties.

To evaluate the influence of the EtOH washing steps used during the preparation of the hybrid materials on the QDs PL emission properties, we have carried out additional PL spectroscopy measurements. Since we used 2 washing steps for the hybrid materials, we evaluated the PL after 2 and 3 precipitation steps with EtOH. Fig. S9 shows that 2 steps do not significantly affect the PL, with a minor PL decrease and a constant PL decay time (suggesting some increased hot exciton trapping or fraction of dark QDs, yet no additional nonradiative losses once the carriers reach the band edge). After 3 steps, we observe a strong PL quenching in both the spectrum and the decay. This concurs with the observation of QDs aggregates in the solution and an increased background in the absorbance spectrum due to Rayleigh scattering. Therefore, we can conclude that the QD PL emission quenching in the QD/rGO hybrid materials is not due to the 2 EtOH washing steps applied, and thus must arise from the interaction between QDs and rGO.

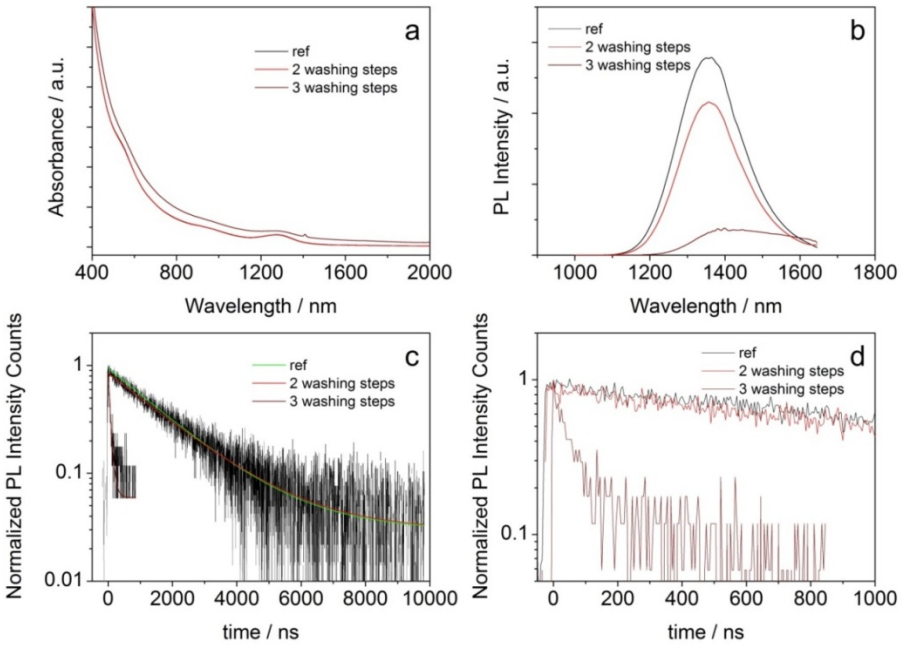

Fig. S9. Absorbance (a) and PL (b) spectra (excitation at 400 nm) of OA-capped PbS QDs (black line) modified by successive washing steps with EtOH dispersed in TCE. PL spectra are normalized to the corresponding absorption (at the excitation wavelength) of the sample. (c, d) The corresponding PL decays (excitation 405 nm, emission 1355 nm) are also shown.

6. Raman characterization.

In order to confirm the reproducibility of the Raman spectra, measurements have been carried out in at least 3 different areas for each sample, obtaining a reliable position of the D and G bands (Fig. S10). In the main text and ESI, all shifts reported correspond to the average obtained from the three spectra.

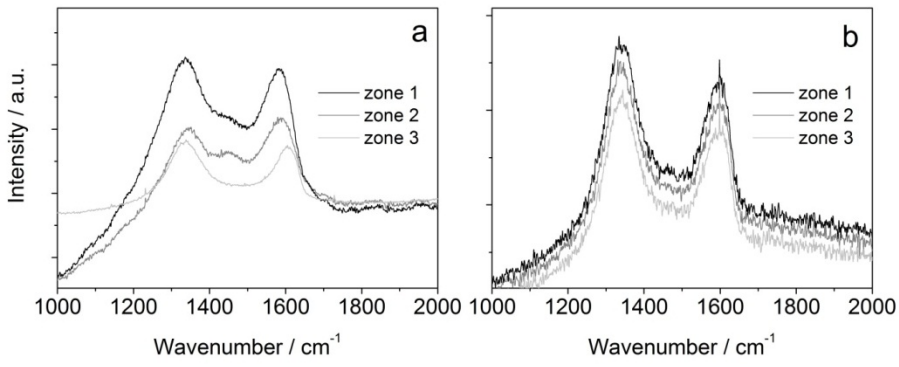

Fig. S10. Comparison between the Raman spectra for different areas of the sample core PbS QD/silane-*f*-rGO (a) and core PbS QD/silane-*f*-GO (b).

From the Raman analysis of the PbS QD/silane-*f*-GO hybrids (Fig. S11) we observed that the silane functionalization of GO leads to a G band upshift of 10 ± 2 cm^{-1}. The attachment of core PbS QDs leads to a downshift of 8 ± 1 cm^{-1} compared with the original silane-*f*-GO spectrum. The shift observed in the case of the GO-based hybrid is lower than for rGO, highlighting the effect of the degree of reduction on the charge transfer process. The Raman shift of the G band can be ascribed to an electron enrichment of the graphene network in PbS QDs-(r)GO hybrid materials and is reduced in the presence of the CdS shell.

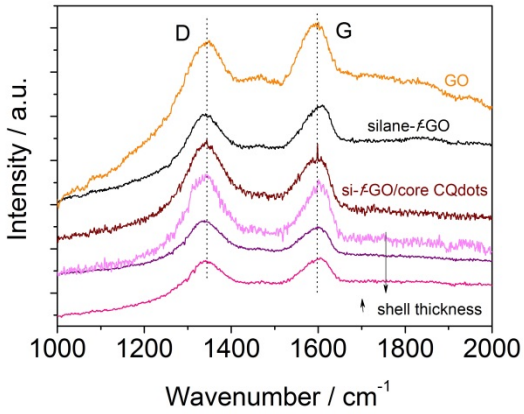

Fig. S11. Comparison between representative Raman spectra of the different core and core-shell PbS/CdS QDs and silane-*f*-GO hybrid samples. In the three lower spectra we systematically varied the shell thickness. The Raman spectrum of the reference material GO is shown as an orange line.

8. PL dynamics in core-shell PbS/CdS QDs and silane-*f*-(r)GO hybrid materials.

Sample	Core diameter (nm)	Shell thickness (nm)	τ_{QD} (μs)	τ_{QD-G} (μs)	η
PbS QDs/silane-*f*-GO	4.98	0	1.4	0.18	0.86
	4.06	0.21	1.2	0.20	0.83
	4.15	0.42	0.90	0.30	0.67
	4.59	0.82	0.72	0.34	0.54
	6.29	0.90	0.36	0.10	0.72
	5.79	1.13	0.28	0.19	0.30
PbS QDs/silane-*f*-rGO	4.98	0	1.4	0.066	0.95
	4.06	0.21	1.2	0.074	0.94
	4.19	0.40	0.66	0.18	0.73
	4.59	0.82	0.72	0.15	0.79
	6.29	0.90	0.36	0.07	0.80

Table S3. PL dynamics data obtained from the time-resolved measurements and Equation 1 (see main text) for the different core-shell PbS/CdS QD/silane-*f*-(r)GO hybrid materials (at the same QD/(r)GO ratio, 0.2 nmol QD per μg (r)GO) prepared in DMF. The efficiency is calculated using the decay time of the corresponding QDs in TCE.

References:

[1] D. R. Dreyer, S. Park, C. W. Bielawski, R. S. Ruoff, *Chem. Soc. Rev.* **2010,** *39*, 228-240.

[2] M. Jahan, Q. Bao, J.-X. Yang, K. P. Loh, *J. Am. Chem. Soc.* **2010,** *132*, 14487-14495.

[3] J. Debgupta, V. K. Pillai, *Nanoscale* **2013,** *5*, 3615-3619.

[4] H. Yang, F. Li, C. Shan, D. Han, Q. Zhang, L. Niu, A. Ivaska, *J. Mater. Chem.* **2009,** *19*, 4632-4638.

[5] Y. Lin, J. Jin, M. Song, *J. Mater. Chem.* **2011,** *21*, 3455-3461.

[6] S. F. Wuister, I. Swart, F. van Driel, S. G. Hickey, C. de Mello Donegá, *Nano Lett.* **2003,** *3*, 503-507.